Antibody-Unfolding and Metastable-State Binding in Force Spectroscopy and Recognition Imaging

Parminder Kaur,[†‡] Qiang-Fu,[†§] Alexander Fuhrmann,[‡] Robert Ros,[‡] Linda Obenauer Kutner,[¶] Lumelle A. Schneeweis,[‖] Ryman Navoa,[¶] Kirby Steger,[¶] Lei Xie,[¶] Christopher Yonan,[¶] Ralph Abraham,[‖] Michael J. Grace,[¶] and Stuart Lindsay[†‡§*]

[†]Biodesign Institute, [‡]Department of Physics, and [§]Department of Chemistry and Biochemistry, Arizona State University, Tempe, Arizona; [¶]Biologic Process and Product Development and [‖]Gene Expression and Protein Biochemistry, Bristol-Myers Squibb, Pennington, New Jersey

ABSTRACT Force spectroscopy and recognition imaging are important techniques for characterizing and mapping molecular interactions. In both cases, an antibody is pulled away from its target in times that are much less than the normal residence time of the antibody on its target. The distribution of pulling lengths in force spectroscopy shows the development of additional peaks at high loading rates, indicating that part of the antibody frequently unfolds. This propensity to unfold is reversible, indicating that exposure to high loading rates induces a structural transition to a metastable state. Weakened interactions of the antibody in this metastable state could account for reduced specificity in recognition imaging where the loading rates are always high. The much weaker interaction between the partially unfolded antibody and target, while still specific (as shown by control experiments), results in unbinding on millisecond timescales, giving rise to rapid switching noise in the recognition images. At the lower loading rates used in force spectroscopy, we still find discrepancies between the binding kinetics determined by force spectroscopy and those determined by surface plasmon resonance—possibly a consequence of the short tethers used in recognition imaging. Recognition imaging is nonetheless a powerful tool for interpreting complex atomic force microscopy images, so long as specificity is calibrated in situ, and not inferred from equilibrium binding kinetics.

INTRODUCTION

The biological utility of atomic force microscopy has been enhanced enormously with the use of antibodies bound to the force-sensing probe by means of a flexible tether (1). This has allowed the binding kinetics between many types of pairs of single molecules to be studied reliably (2). The technique was extended to chemically sensitive imaging using electronics that detects binding events as a topographical image is acquired (3), yielding simultaneous maps of sample topography and chemical composition with nanometer-scale resolution. This allows for identification of particular proteins (4) or other molecules, like sugars (5), something that was previously extremely difficult to do in high-resolution images. Optimal conditions for recognition imaging as well as sources of error in the (simultaneously-acquired) topographical image were reviewed recently (6).

Recognition imaging can be limited by the performance of antibodies, which are often significantly less selective in this application than their equilibrium binding constants imply (7,8). We have developed DNA aptamers as recognition molecules in an attempt to address this problem. They are better than antibodies in some applications, but still suffer from reduced selectivity relative to that measured from their on-target and off-target equilibrium binding constants (8–10).

The effective molar concentration, C, of an antibody tethered to a probe by a linker of a few nm length is ~15 mM. For a binding event to occur, the antibody must stay over the target for time given by $t_{on} \sim (K_{on}\ C)^{-1}$. For a typical atomic force microscopy (AFM) linear scan rate of 1 μm/s, we require $t_{on} < 1$ ms, or $K_{on} > 0.015\ M^{-1}\ s^{-1}$. This is many orders-of-magnitude less than typical diffusion-limited on-rates, so, even at fast scan speeds, antibodies on the probe will find, and bind, to their target. Once the bound complex is formed, it will stay bound if the probe remains over the target for a time $\geq (K_{off})^{-1}$, a condition that is easily met for strong interactions where $K_{off} \geq 10^{-3}\ s^{-1}$. Of course, the complex is pulled apart once an adequate force is generated by the lateral scanning motion of the AFM probe. The result is a "recognition image spot" of approximately twice the tether length in diameter.

In a surprising discovery, van Es (11) examined recognition images between a biotinylated target and a streptavidin probe, finding evidence of unbinding and rebinding on ms timescales. Because the dissociation constant, K_D, for this complex is ~10^{-15} M, unbinding on a millisecond timescale appears to be inconceivable. We show in this article that we also see evidence of unbinding events in ~80% of the recognition events between an antibody and target for which the equilibrium dissociation constant is measured to be ~10^{-11} M. Force spectroscopy shows that partial unfolding of the antibody occurs frequently at high loading rates. This propensity to unfold depends on the probe history—an antibody previously exposed to high loading rates is more likely to unfold at low loading rates. The effect is also

Submitted September 27, 2010, and accepted for publication November 23, 2010.

*Correspondence: stuart.lindsay@asu.edu

Editor: Denis Wirtz.

0006-3495/11/01/0243/8 $2.00

doi: 10.1016/j.bpj.2010.11.050

reversible—continued use at low loading rates restores stability to the antibody. This implies that exposure to high loading rates induces a transition to a metastable state that is more readily unfolded. Because the loading rates in recognition imaging are always high, the antibody is likely to be mostly in this metastable state, accounting for the loss of specificity. Thus, chemically stabilized recognition elements (12) might improve the specificity of the technique.

MATERIALS AND METHODS

Reagents

Recombinant human monoclonal anti-IgG, a highly purified monovalent Fab fragment and the targeted receptor, were produced in-house at Bristol-Myers Squibb (Hopewell, New Jersey) from mammalian cell culture. The Fab fragment was prepared from the intact monoclonal anti-IgG molecule. The anti-IgG receptor was purified from a mammalian cell culture using Protein A affinity chromatography, and polished in a Superdex 75 resin column (GE Healthcare, Piscataway, NJ). All materials were >95% pure when tested by high-performance liquid chromatography using analytical size exclusion chromatography with a TSK 3000 SWXL column (Tosoh Bioscience, King of Prussia, PA).

Recognition imaging

APTES (3-Aminopropyltriethoxysilane) glutaraldehyde-functionalized mica surfaces were freshly prepared as described earlier (13). Fifteen microliters of receptor (diluted to 0.5 ng/μL in phosphate-buffered saline (PBS)) was pipetted onto the APTES-GD mica surface. The surface was allowed to stand for 50 min and was later rinsed with PBS buffer and loaded into the AFM liquid cell for imaging under MAC mode. Solutions of 10 ng/μL were used for force curves to achieve a higher surface coverage. The AFM probe was functionalized with the bivalent IgG or monovalent Fab and the surface with the receptor.

Cantilevers were ultraviolet-cleaned using an ultraviolet ozone cleaner for 15 min and coated for Mac Mode operation. The cantilevers were introduced into a desiccator containing a few drops of freshly distilled APTES (Sigma-Aldrich, St. Louis, MO) in a water-free argon environment, and left for 50 min. One milligram of MAL-PEG 24-NHS ester (MW = 1395, fully stretched length = 9.52 nm; Quanta BioDesign, Powell, OH) was dissolved in 500 μL of chloroform to which was added 5 μL of triethylamine. The APTES-treated cantilevers were rinsed with chloroform and then dipped into the solution containing the linker for 2–3 h.

The bivalent IgG or monovalent Fab was thiolated as follows: A solution of 1 mg/mL of IgG was washed in buffer A (100 mM NaCl, 50 mM NaH_2PO_4, 1 mM EDTA, pH 7.5) on a PD10 column and a 10-fold molar excess of SATP in DMSO added to the fractions containing antibody. The samples were left for 1 h under argon at room temperature, and the samples were again washed with buffer A on a PD10 column. Probes functionalized with MAL-PEG-NHS were washed with chloroform and were dried with argon, and drops of 50 μL SATP-treated antibody solution plus 25 μL NH_2OH in 50 μL buffer A (150 mM NaCl, 50mM Na_2HPO_4, pH 7.5) were placed onto each probe and left for 1 h. The tips were washed with buffer A, and then PBS buffer and were stored in PBS buffer at 4°C.

The probe and sample were mounted on a Pico SPM I scanning probe microscope (Agilent Technologies, Chandler, AZ), and topographic and recognition imaging with force measurements were carried out under PBS buffer solution. We used silicon nitride probes with nominal spring constant 0.1 N/m (Veeco Instruments, Plainview, NY) and nominal spring constant 0.08 N/m (Olympus, Melville, NY). Individual probes were calibrated using the thermal noise method. Recognition images were usually acquired at a peak-to-peak amplitude of 8.3 nm (though the effects of changing amplitude were also studied) and a scan rate of 1.5 lines/s using PicoTREC electronics (Agilent).

For both recognition images and force curves, specificity was tested by attaching a matching isotype antibody on the cantilever and obtaining no recognition or binding to the covalently captured receptor, and confirmed by blocking the recognition images with free monoclonal IgG flowed into the sample cell (see Fig. S1 and Fig. S2 in the Supporting Material). Recognition events were counted when the voltage level fell below the thermal noise level on the background signal as described by Lin et al. (10). The background and its range were determined from the entire background in each leveled image with recognition spots excluded. We sampled >1800 recognition spots taken from ~100 images. Of these spots, 1500 showed the switching noise discussed below, whereas ~300 showed continuous recognition on each line of the recognition spot.

Force spectroscopy

Force spectroscopy was carried out with a MFP3D AFM (Asylum Research, Santa Barbara, CA). We used the same silicon nitride AFM probes and mica surfaces were functionalized as described above, and force curves acquired in the same conditions used for recognition imaging. The probe was brought into gentle (repulsive force < 30 pN) contact for 0.2 s and force curves obtained as the probe was retracted at speeds between 25 and 5000 nm/s. Data were analyzed using automated software to select curves that started at the baseline (zero force) and showed a single rupture event after a retraction of ~9 nm (see the *inset* later in Fig. 3 *A*) (14,15). Polynomial fits to the extension curves were dominated by the linear term, from which the spring constant of the system of cantilever and PEG tether was found to be 24 $\pm$ 5 pN/nm.

Surface plasmon resonance

Equilibrium binding constants were determined by kinetic analysis using surface plasmon resonance (SPR) detection with a Biacore T100 instrument (GE Healthcare). Recombinant receptor was diluted to 2 μg/mL into 10 mM sodium acetate (pH 4.5) and injected over one or more flow cells of a CM5 biosensor chip to produce antigen densities of ~200 RU. All surfaces were subsequently blocked with 1 M ethanolamine. All binding experiments were performed at 25°C using HBP EP+ (10 mM HEPES, 150 mM NaCl, 3 mM EDTA, 0.05% surfactant P20 at pH 7.4) as running buffer. The bivalent IgG and monovalent Fab fragment were injected for 180 s at a flow rate of 5 μL/min and dissociation monitored for 3600 s.

The antigen surfaces were regenerated with a 30-s pulse injection of 10 mM glycine pH 1.5 for 30 s at a 60 μL/min flow rate. The bivalent IgG was diluted into HPS EP+ buffer. The monovalent Fab fragment was prepared the same way. The concentrations tested for the whole IgG and purified Fab fragment were empirically derived and ranged from 0.11 nM to 10 nM and 0.16 nM to 20 nM, respectively. Response data were processed using a reference surface to correct for bulk refractive index changes and any nonspecific binding. Data were also double-referenced using responses from blank injections. To determine the antibody sample/antigen binding constants, association and dissociation phase kinetic data from the antigen surfaces were fitted to a 1:1 Langmuir binding model using Biacore T100 evaluation software (GE Healthcare). Results are tabulated in Table 1.

RESULTS AND DISCUSSION

Typical examples of topographic and recognition images are shown, respectively, in Fig. 1, *A* and *B* (further examples are given in Fig. S1). The target receptor is ~10 nm in diameter and isolated molecules (as well as three larger aggregates) are clearly seen in this image. The recognition image

TABLE 1 On- and off-rates

Sample	K_{on} (1/Ms)	K_{off} (1/s)	K_D (M)	χ^2 (RU^2)
Kinetics of antibody binding using SPR				
Whole IgG	$7.57 \times 10^{+5}$	4.19×10^{-5}	5.53×10^{-11}	0.219
	$4.21 \times 10^{+5}$	2.88×10^{-5}	6.85×10^{-11}	0.715
Fab	$1.39 \times 10^{+6}$	6.93×10^{-3}	5.00×10^{-9}	0.36
	$4.71 \times 10^{+5}$	3.02×10^{-3}	6.40×10^{-9}	0.30
Kinetics of antibody binding from recognition image noise				
Whole IgG	$8 \pm 1 \times 10^{3}$	$2.1 \pm 0.3 \times 10^{2}$	0.1 ± 0.1	

Rates were determined by Biacore SPR (GE Healthcare) for the whole IgG and the Fab fragment and for the whole IgG by recognition imaging switching noise.

(Fig. 1 *B*) shows a dip in the top displacement of the probe (*dark spots*) associated with each feature in the topography. Because these spots were abolished when free antibody was flowed into the liquid cell (Fig. S1) and were not observed when a probe functionalized with a matching isotype antibody was used (Fig. S2), the interactions are clearly specific. Nonetheless, close examination of the recognition spots shows rapid unbinding signals that are very similar to those first reported for biotin-streptavidin by van Es (11). We found these events in 80% of the recognition images. The remaining 20% showed no sign of transient unbinding. A blown-up recognition spot is shown in Fig. 1 *C* to illustrate typical unbinding events, circled in the image. Here the contrast has been adjusted so that the surrounding background is white.

This noise in the image can be used to measure the on (t_{on}) and off (t_{off}) times directly, as illustrated in Fig. 1 *D*. The duration of a line scan up to the point of an internal (*circled events*) unbinding event, i.e., before the antibody is pulled off, gives a value for t_{on}. The time to rebind gives a value for t_{off}, a quantity not previously available from force spectroscopy.

An immediate concern arises from the possibility that the unbinding events represent nothing more than thermal noise on the recognition signal. Fig. 1 *E* shows the distribution of signal levels for pixels in the bound region (i.e., dark parts of spots; *solid histogram bars*), the transiently unbound regions (*open histogram bars*; mostly obscured) and the surrounding area (*shaded bars*). The signals from the transiently unbound regions and the surrounding background are essentially the same, whereas signals in the bound regions are significantly lower.

A statistical analysis of some 1500 events yields the distributions of off- and on-times shown in Fig. 2, *A* and *B*. The solid lines are fits to a Gaussian plus a constant background. From these fits, $t_{off} = 4.8 \pm 0.8$ ms and $t_{on} = 9 \pm 0.2$ ms, but with a significant fraction of even longer times, as indicated by the constant background in Fig. 2 *B*. The modal value of t_{off} gives K_{off} directly as 2.1×10^2 s^{-1}. To interpret t_{on} we need an estimate of the effective concentration of the antibody on the probe. The PEG linker consists of 24 units each of 0.34 nm, which we will assume to be freely-jointed, leading to an end-to-end length of 1.9 nm.

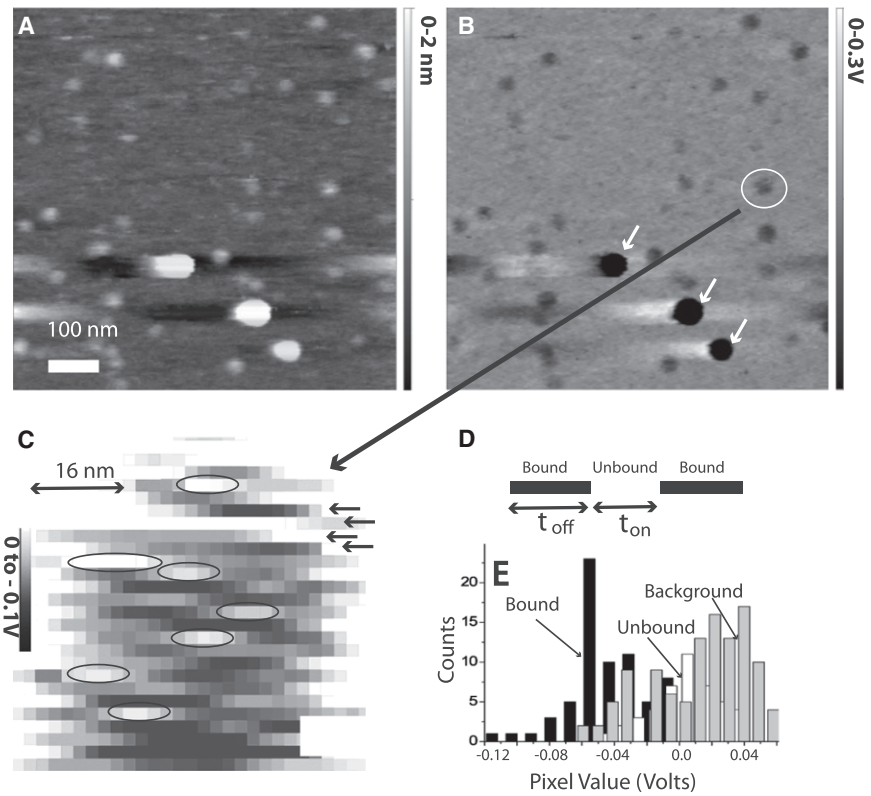

FIGURE 1 Unbinding events in recognition images: (*A*) Topographic images of receptors on an activated mica surface. (*B*) Simultaneously acquired recognition image. (*Dark spots*) Regions where the antibody on the tip is bound to the target on the surface. (*White arrows*) Interactions with large aggregates. (*C*) Blow-up of a recognition spot showing the switching noise observed in 80% of the spots. An unbinding event occurs at end of each scan line where the background goes to white (scan direction is *left* to *right*). Only scan lines with unbinding events within the spot are circled, and these are used to determine t_{on} and t_{off}. Other scan lines (some are pointed to with *arrows*) show no internal unbinding events. The background voltage level has been set equal to zero. (*D*) Interpretation of the fluctuations in the line-scan recognition signal in terms of binding and unbinding times. The length of time for which the antibody remains bound determines t_{off} while the time to rebind determines t_{on}. The duration of the second binding event is controlled by the forced detachment of the antibody. (*E*) Histogram of voltage levels in the recognition events. (*Solid bars*) Data for the bound states, (*open bars*) data for the unbound states, and (*shaded bars*) data for the background adjacent to the recognition spot. The on-off events correspond to level changes greater than the intrinsic noise in the image. The background has been set equal to zero.

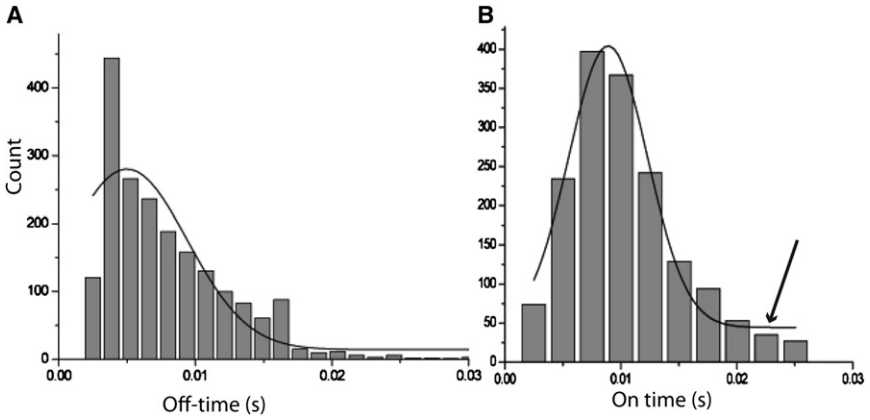

FIGURE 2 Distribution of on- and off-times from recognition images. (*A*) Distribution of times for coming off after a binding event and (*B*) distribution of times for rebinding after an unbinding event. (*Solid lines*) Fits to a Gaussian yielding $K_{off} = 208 \pm 30\ s^{-1}$. The on-time data are fitted by a Gaussian yielding $t_{on} = 9 \pm 1.6$ ms, but a constant background (*arrow* in *B*) shows a broad distribution of much longer on-times. Assuming a local concentration of 0.015 M yields $K_{on} = 8 \times 10^3\ M^{-1}\ s^{-1}$.

With a peak amplitude of 8.3 nm, we estimate that the antibody occupies a cylindrical volume of 94 $(nm)^3$ or 10^{-22} L. This yields an effective concentration of ~15 mM. This is probably a significant underestimate, because binding is more likely to occur at the bottom of the cantilever oscillation when the effective concentration will be even greater. However, using this value yields $K_{on} = 8 \times 10^3\ M^{-1}\ s^{-1}$. These data are listed alongside data obtained from the Biacore T100 SPR data in Table 1. The off-rate measured in the recognition images is six-orders-of-magnitude faster than the equilibrium rate. The on-rate is also reduced significantly, the direction of likely errors in the concentration increasing this discrepancy.

Force spectroscopy yields some insight into these discrepancies. We compiled histograms of the bond-breaking force at each retraction speed, from which the modal bond-breaking force was derived. In our first analysis, we retained single-rupture events of up to 20 nm in extent. This is significantly longer than the extended tether length (of 9.5 nm), but most pull lengths appeared to be clustered in this range and the uncertainties in the point of contact justify some latitude. The loading rate was calculated as the product of the retraction speed and the effective force constant of the tether/cantilever system (24 pN/nm). A plot of modal bond-breaking force versus the natural logarithm of the loading rate is shown in Fig. 3 *A* with the error bars representing ± 1 SD on the force distributions. The spread in the data increases by a large amount for values of the log of the loading rate above 10.

The number of long pulls (length> 20 nm) increased at higher loading rates, so we analyzed the distribution of these lengths for all sets of data. Some representative examples are shown in Fig. 4, *A–C*. Particularly at low loading rates (retraction speeds of 500 nm/s or less) the distribution of pull lengths was well fitted by a single Gaussian with a peak near the fully stretched length of the PEG tether (Fig. 4 *A*; loading rate is 12,000 pN/s). These data were taken with four different probes and the width reflects the possibility of different binding sites on the probe as well as different lateral alignments between the probe and the target molecule on the surface. At high loading rates (Fig. 4 *C*; loading rate is 48,000 pN/s), multiple peaks were often (but not always) seen in the length distribution. Additional peaks were also seen at low loading rates if the

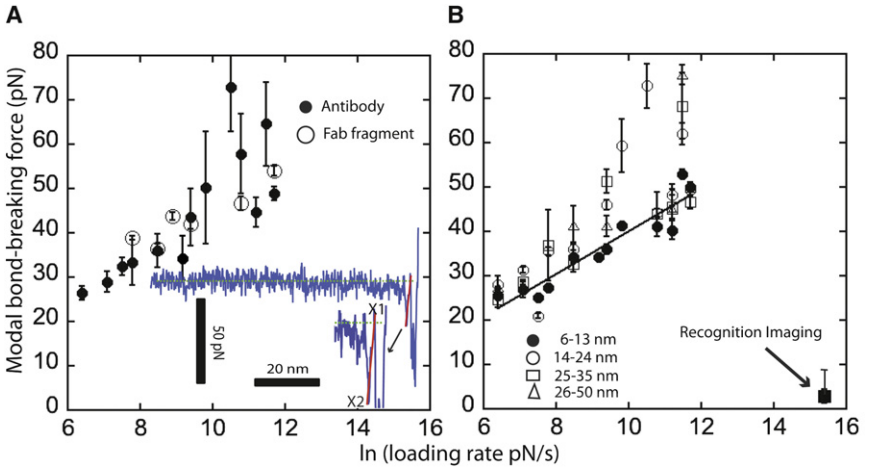

FIGURE 3 Evans plots for force spectroscopy data. (*Inset* in *A*) Typical unbinding curve; the line (*red* in the *online version*) is an automatic fit to the pulling event detected by the software; the pulling length is the horizontal distance between the start of the pull (X1) and the end of the pull (X2). (*A*) Modal force for unbinding versus natural log of loading rate for the bivalent IgG antibody (*solid circles*) and the monovalent Fab (*open circles*). (*B*) Same as in panel *A*, but data are analyzed in groups according to the pulling lengths as shown by the legend. (*Solid line*) Fit of the Evans theory to those points (*solid circles*) that have a pulling length (~9 nm) indicative of no unfolding of the antibody or its target receptor. (*Square datum*, *lower right*) Recognition imaging unbinding events.

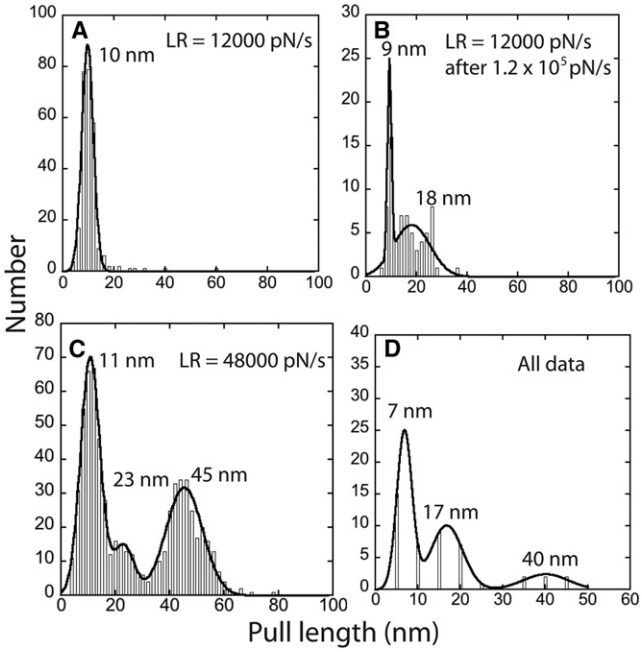

FIGURE 4 Distribution of pulling lengths showing how high loading rates drive unfolding. (*A*) At 500 nm/s retraction speed, the pull-lengths are distributed tightly around the 9.5-nm length of the PEG tether. (*B*) After the probe was used at 5000 nm/s retraction rate, (*C*) data taken at 500 nm/s shows a new feature in the length distribution at ~18 nm, indicating that an additional 8–9 nm of antibody is more likely to unfold. (*D*) Example of a run at 2000 nm/s where unfolding occurs at several lengths. (*E*) Summary of peaks positions in fits to 40 sets of data like those shown in panels *A–C*. Unfolding of 8 nm of antibody (~20 amino acids) is quite likely. Because the propensity to unfold reduces with time after the loading rate is reduced, the antibody likely undergoes a metastable structural transition at high loading rates.

probe had previously been used at high loading rates. An example is shown in Fig. 4 *B* (loading rate = 12,000 pN/s), where an additional peak near 18 nm has developed after the probes was previously loaded at 1.2×10^5 pN/s for a few hundred pulls. This suggests that, although unfolding of the target is possible, it also occurs in the antibody on the probe, because the behavior of the probe reflects its history. The process is generally reversible, the length distribution returning to one like that in Fig. 4 *A* after a few hundred pulls at low loading rate.

Fig. 4 *D* shows the distribution of peak values obtained by fitting some 40 distributions like those shown in Fig. 4, *A–C*. The feature at 17 nm is quite common, suggesting that a particular region of the antibody is prone to unfolding. The net length (17–9.5 nm = 7.5 nm) corresponds to ~20 amino-acid residues (16), which is a small fraction of any of the chains composing the antibody.

With this insight, we have analyzed single-rupture events with pull-lengths falling into each of the regions of unfolding lengths (the region from 25 to 50 nm was split into two groups) and these data are shown in Fig. 3 *B*. Clearly, the large spread of modal breaking forces is owing to events in which the antibody (and possibly the target) partially unfolds.

As a first approximation for obtaining the thermal off-rate and potential barrier width (also known as reaction length, x_β, i.e., the difference between the maximum of the potential barrier and the minimum of the metastable state along the reaction coordinate) we used the standard method of Evans and Ritchie (17). The solid line in Fig. 3 *B* is a fit to this theory of in which the modal unbinding force is given by

$$f_p = \frac{k_B T}{x_\beta} \ln\left[\frac{r x_\beta}{k_B T K_{off}}\right],$$

where r is the loading rate in *N*/s, x_β the distance to the transition state in meters, and $k_B T$ is the thermal energy in Joules. Thus, the slope of the plot yields $\frac{k_B T}{x_\beta}$ and the intercept yields

$$\frac{k_B T}{x_\beta} \ln\left[\frac{x_\beta}{k_B T K_{off}}\right].$$

The slope yields x_β directly, whereas K_{off} is obtained from the slope and the exponential of the ratio of the slope to the intercept. We find $x_\beta = 0.83$ nm and $K_{off} = 0.24\ s^{-1}$.

We now turn to a more sophisticated analysis of these data. Because the changes of the loading force on the bond molecules are rather slow in comparison to molecular relaxation processes, the reaction kinetics can be approximated by

$$\frac{dn(t)}{dt} = -K_{off}(f(t))n(t), \quad (1)$$

where $n(t)$ denotes the survival probability of the bond at a given time t. Assuming that the force as function of time $f(t)$ depends solely on the total extension, $s = vt$, of all elastic components (molecules, linker, cantilever, etc.) which leads to

$$F(s) = F(v \cdot t) = f(t), \quad (2)$$

where $F(s)$ is independent of the pulling velocity v. With Eq. 1, the formal solution of the survival probability of the bond under an externally applied force f for any $K_{off}(f)$ and $F(s)$ is given by Raible et al. (18) as

$$n_v(f) = \exp\left\{-\frac{1}{v}\int_{f_{min}}^{f} df' \frac{K_{off}(f')}{F'\left(F^{-1}(f')\right)}\right\}, \quad (3)$$

with $nv(f(t)) = n(t)$ and $n(t=0) = nv(f = f_{min}) = 1$. Here, f_{min} is the threshold value below which dissociation forces cannot be distinguished from thermal fluctuations. Additionally, it is assumed that the increase in the loading force is strictly monotonic, so that the inverse function F^{-1} of $F(s)$ exists. Starting from the survival probability of the bonds $nv(f)$ at pulling velocity v (Eq. 3), a function $g(f)$ can be defined as

$$g(f) = -v \ln n_v(f). \quad (4)$$

Under the assumptions of Eqs. 1 and 2, this $g(f)$ should be independent of the pulling velocity.

Fig. 5 *B* shows a plot of all rupture force data for the different pulling velocities. It is obvious that these data are not independent of v. This was observed before (19,20). A model, which describes our data more precisely is the so called heterogeneous bond model (18). This model is an extension of the standard theory. The parameter x_β (reaction length) itself is, in this model, subjected to random variations. This reflects statistical and uncontrollable variations of the molecular complex or of the local environment of the bond. The parameter x_β is sampled from a Gaussian distribution with mean x_β and variance σ_x^2. The heterogeneous bond model thus involves the three parameters x_β, σ_x, and K_{off}.

Fig. 5 *A* shows a selection of the rupture force distributions with the solid lines showing results of the heterogeneous bond model with the parameters given in Table 2 (21). The parameters obtained from these fits (listed in Table 2) were used to predict the bond-breaking probabilities as a function of force and pulling speed. These predictions are shown by the solid lines in Fig. 5 *B*. The relatively good agreement (factor 2 in K_{off}, good agreement for x_β) between the results of an analysis using the Evans model and that of the heterogeneous bond model lend confidence that the derived value of K_{off} is not greatly distorted by the method of analysis.

TABLE 2 Off-rate and distance to the transition state (x_β)

Parameter	Evans-Ritchie	Heterogeneous bond model
x_β	0.83 nm	0.85 ± 0.03 nm
K_{off}	0.24 s^{-1}	0.092 ± 0.06 s^{-1}
	(t_{off} = 4.2 s)	(t_{off} = 31 to 6.5 s)
Width of x distribution		0.41 ± 0.025 nm

IgG binding events were determined from force spectroscopy analysis of the data with pull-lengths in the range 6–13 nm for the Evans theory and the heterogeneous bond model. Heterogeneous bond model also yields a width of the distribution of x_β.

The values of K_{off} derived from both the Evans model and the heterogeneous bond model (Table 2) differ from the SPR results (Table 1) by four orders of magnitude (and from the off-rate implied by recognition imaging by yet another three orders of magnitude). SPR data can underestimate K_{off} because of errors caused by rebinding (22), though in one case where SPR and force spectroscopy data have been compared directly in the past, the discrepancy was not large (23).

One explanation for the discrepancy between the kinetics observed in force spectroscopy and the kinetics measured by SPR lies in the initial binding process, the available orientations of ligand and receptor being somewhat more limited in the AFM geometry. Because one might reasonably expect that the binding process of the antibody and one of its arms (the Fab fragment) would be different, we chose to compare Fab binding to that of the whole antibody. SPR data (Table 1) shows that the Fab fragment both binds more rapidly (by a factor 10×) and releases its target more rapidly (by a factor

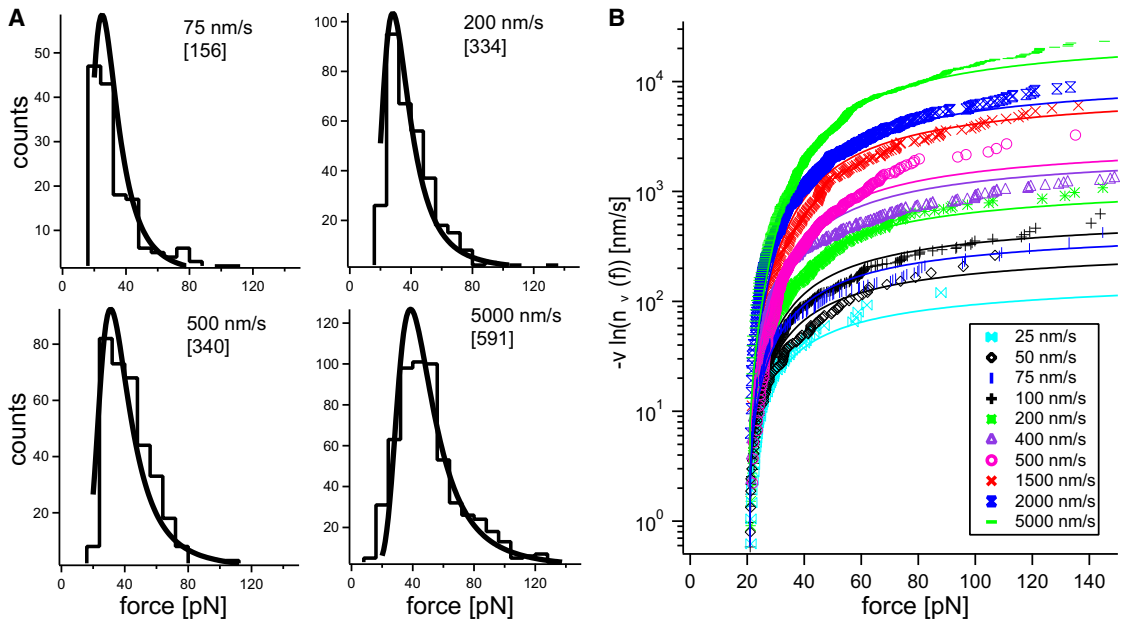

FIGURE 5 Fits of the full data set for IgG unbinding to the heterogeneous bond model for pulling lengths in the range of 9–13 nm. (*A*) Histograms of bond-breaking forces at the pulling speeds marked. (*Solid lines*) Maximum likelihood fits to the heterogeneous bond model. (*B*) Bond survival probability plotted versus bond-breaking force for pulling speeds from 25 to 5000 nm/s as marked (*color-coded* in the *online version*). (*Solid lines*) Fits using the same heterogeneous bond model parameters. These fits yield a zero-force off rate of 0.092 s^{-1}.

100×) than the intact antibody. However, in force spectroscopy (*open circles* in Fig. 3 *A*), the Fab fragment behaves much like the intact antibody (*solid circles* in Fig. 3 *A*). This suggests that, in the AFM experiments, only one arm of the antibody is binding the target, perhaps as a result of steric constraints imposed by the tethering PEG molecule. Thus, K_{off} as measured for the Fab fragment is more favorably compared to the AFM data.

The lower bound on the value derived from force spectroscopy using the heterogeneous bond model ($K_{off} = 32 \times 10^{-3}$ s^{-1}) is within an order of magnitude of the values derived from SPR for the Fab fragment ($K_{off} = 7$ to 3×10^{-3} s^{-1}). This is still a significant discrepancy, one that seems unlikely to be accounted for by rebinding in SPR measurements (22). Using much longer (34 nm) PEG tethers, one on the target and one on the an antibody single Fv fragment, Morfill et al. (24) found good quantitative agreement between SPR and force spectroscopy data. This suggests that geometry used in recognition imaging—one short PEG tether with a target fixed directly to a solid surface—inhibits formation of a properly bound complex.

This leaves us with the issue of the much larger discrepancy between the rapid off times derived from the recognition imaging signals and those inferred from force spectroscopy. These are three-orders-of-magnitude higher ($K_{off} = 2.1 \times 10^{2}$ s^{-1}) than the upper bound obtained from force spectroscopy ($K_{off} \leq 1.52 \times 10^{-1}$ s^{-1}). This discrepancy is cast into sharp relief by plotting the recognition bond-breaking events on the Evans plot (Fig. 3 *B*). To do this, we estimated the loading rate used in recognition imaging as follows: The velocity of the probe is given by $2\pi Af \cos(2\pi ft)$ giving a maximum value of $2\pi Af$ where A is the half-amplitude (4 nm) and $f = 8.4$ kHz. Taking the spring constant to be 24 pN/nm yields a loading rate of 2×10^{5} pN/s. (We have not characterized the combination of PEG tether and the cantilevers used for recognition imaging, but an upper limit is set by the largest spring constant of the cantilevers themselves, 100–80 pN/nm, a difference not noticeable on this log scale.)

We can estimate the bond-breaking force from the dip in amplitude multiplied by the effective spring constant of the system. Calibration of the TREC electronics shows that the peak dip in amplitude signal (Fig. 1 *E*) corresponds to 0.12-nm amplitude reduction, or a force of 2.9 pN (the *y* axis error bar on the data point (*solid square*, Fig. 3 *B*) reflects the upper bound set by choosing the largest cantilever stiffness to calculate the force). It is clear that the unbinding in recognition imaging reflects a completely different process from the binding events (*solid circles* in Fig. 3 *B*) or the unfolding events (*open symbols* in Fig. 3 *B*). Because we have established that unfolding occurs quite commonly at the higher loading rates, the most likely explanation is that the switching noise in recognition imaging stems from interactions between partially unfolded parts of the antibody and the target receptor. These interactions are not nonspecific (as demonstrated by the control experiments; see the Supporting Material) but generate binding forces too weak to be detected at the normal loading rates used in force spectroscopy, as can be seen by inspection of Fig. 3 *B* and the noise levels in a typical force curve (*inset*, Fig. 3 *A*). Linear extrapolation of the force (assuming a similar slope to that in the force spectroscopy) from the recognition imaging datum down to loading rates used in force spectroscopy would result in modal unbinding forces smaller than the thermal noise in the system. Thus, the events that produce the recognition spots are not seen at all in force spectroscopy.

Finally, we tested the effect of changing the oscillation amplitude on the measured on- and off-rates obtained from the switching observed in recognition images. Over the maximum range that gave recognition signals (9.5–6.5 nm, peak to peak), we found no significant changes in the distributions of either t_{on} or t_{off}.

CONCLUSIONS

In summary, we have shown that binding in force spectroscopy is affected significantly by partial unfolding of the antibody at higher loading rates, a significant fraction of the pulls reflecting partial unfolding of the antibody. Because this propensity to unfold can be inherited by running the probe at high loading rates for a while, it suggests that the antibody refolds into a metastable state that is more likely to unfold. The process is reversible, because the unfolding stops after a number of runs at the lower loading rate. When the distribution of measured pull-lengths is used to select data from events in which the antibody remains intact, the measured binding kinetics is within an order of magnitude of those obtained from SPR data for the Fab fragment, implying that only one arm of the antibody usually binds in the force spectroscopy experiment.

The on-rate obtained from recognition imaging is much slower yet, likely also a consequence of the formation of a metastable conformation of the antibody in the high-loading rate regime. At the loading rates used for recognition imaging, the interactions are very much weaker in most (80%) of the binding events, reflecting a preponderance of interactions with the antibody in the metastable state in which unfolding is more likely. The specificity of recognition imaging should be greatly enhanced by the use of more rigid recognition reagents, such as the recently introduced cyclotides (12). Until better recognition reagents are developed, the presence of switching noise in the recognition spots can be used to reject data arising from weakly bound receptor-ligand pairs.

SUPPORTING MATERIAL

Two figures are available at http://www.biophysj.org/biophysj/supplemental/S0006-3495(10)01477-3.

We are grateful to Terjk Oosterkamp and Peter Hinterdorfer for pointing out the earlier work of van Es and for comments on an earlier version of this manuscript. We thank Reb Russell, Ralph Abraham, and Alan Flesher for useful discussions.

R.R., A.F., and S.L. were supported in part by a grant from the National Cancer Institute (grant No. U54CA143682).

REFERENCES

1. Hinterdorfer, P., W. Baumgartner, …, H. Schindler. 1996. Detection and localization of individual antibody-antigen recognition events by atomic force microscopy. *Proc. Natl. Acad. Sci. USA.* 93:3477–3481.
2. Greenleaf, W. J., M. T. Woodside, and S. M. Block. 2007. High-resolution, single-molecule measurements of biomolecular motion. *Annu. Rev. Biophys. Biomol. Struct.* 36:171–190.
3. Stroh, C., H. Wang, …, P. Hinterdorfer. 2004. Single-molecule recognition imaging microscopy. *Proc. Natl. Acad. Sci. USA.* 101:12503–12507.
4. Hinterdorfer, P., and Y. F. Dufrêne. 2006. Detection and localization of single molecular recognition events using atomic force microscopy. *Nat. Methods.* 3:347–355.
5. Wang, H., L. Obenauer-Kutner, …, S. M. Lindsay. 2008. Imaging glycosylation. *J. Am. Chem. Soc.* 130:8154–8155.
6. Preiner, J., A. Ebner, …, P. Hinterdorfer. 2009. Simultaneous topography and recognition imaging: physical aspects and optimal imaging conditions. *Nanotechnology.* 20:215103.
7. Bash, R., H. Wang, …, D. Lohr. 2006. AFM imaging of protein movements: histone H2A-H2B release during nucleosome remodeling. *FEBS Lett.* 580:4757–4761.
8. Lin, L., Q. Fu, …, S. Lindsay. 2009. Recognition imaging of acetylated chromatin using a DNA aptamer. *Biophys. J.* 97:1804–1807.
9. Lin, L., D. Hom, …, J. C. Chaput. 2007. In vitro selection of histone H4 aptamers for recognition imaging microscopy. *J. Am. Chem. Soc.* 129:14568–14569.
10. Lin, L., H. Wang, …, S. Lindsay. 2006. Recognition imaging with a DNA aptamer. *Biophys. J.* 90:4236–4238.
11. van Es, M. H. 2008. A new touch to atomic force microscopy: smart probing of biological and biomedical systems at the nanoscale. PhD thesis. University of Leiden, Leiden, Belgium.
12. Jagadish, K., and J. A. Camarero. 2010. Cyclotides, a promising molecular scaffold for peptide-based therapeutics. *Biopolymers.* 94:611–616.
13. Wang, H., R. Bash, …, S. M. Lindsay. 2002. Glutaraldehyde modified mica: a new surface for atomic force microscopy of chromatin. *Biophys. J.* 83:3619–3625.
14. Fuhrmann, A., D. Anselmetti, …, P. Reimann. 2008. Refined procedure of evaluating experimental single-molecule force spectroscopy data. *Phys. Rev. E Stat. Nonlin. Soft Matter Phys.* 77:03912–03922.
15. Fuhrmann, A. 2010. Force spectroscopy, from single molecules to whole cells: refined procedures of data analysis. PhD thesis. Arizona State University, Tempe, AZ.
16. Rief, M., M. Gautel, …, H. E. Gaub. 1997. Reversible unfolding of individual titin immunoglobulin domains by AFM. *Science.* 276:1109–1112.
17. Evans, E., and K. Ritchie. 1997. Dynamic strength of molecular adhesion bonds. *Biophys. J.* 72:1541–1555.
18. Raible, M., M. Evstigneev, …, P. Reimann. 2006. Theoretical analysis of single-molecule force spectroscopy experiments: heterogeneity of chemical bonds. *Biophys. J.* 90:3851–3864.
19. Raible, M., M. Evstigneev, …, R. Ros. 2004. Theoretical analysis of dynamic force spectroscopy experiments on ligand-receptor complexes. *J. Biotechnol.* 112:13–23.
20. Fuhrmann, A., J. C. Schoening, …, R. Ros. 2009. Quantitative analysis of single-molecule RNA-protein interaction. *Biophys. J.* 96:5030–5039.
21. Getfert, S., and P. Reimann. 2007. Optimal evaluation of single-molecule force spectroscopy experiments. *Phys. Rev. E Stat. Nonlin. Soft Matter Phys.* 76:052901–052905.
22. Gopalakrishnan, M., K. Forsten-Williams, …, U. C. Täuber. 2005. Ligand rebinding: self-consistent mean-field theory and numerical simulations applied to surface plasmon resonance studies. *Eur. Biophys. J.* 34:943–958.
23. Fuhrmann, A., and R. Ros. 2010. Single-molecule force spectroscopy: a method for quantitative analysis of ligand-receptor interactions. *Nanomedicine (Lond).* 5:657–666.
24. Morfill, J., K. Blank, …, H. E. Gaub. 2007. Affinity-matured recombinant antibody fragments analyzed by single-molecule force spectroscopy. *Biophys. J.* 93:3583–3590.